A Low-Dimensional Dynamical Model for the Solar Wind Driven Geotail-Ionosphere System

W. Horton

Institute for Fusion Studies, The University of Texas at Austin

Austin, Texas 78712 USA

and

I. Doxas

University of Colorado, Boulder, CO 80309

August 21, 1997

Abstract

A six-dimensional nonlinear dynamics model is derived for the basic energy components of the night-side magnetotail coupled to the ionosphere by the region 1 currents. In the absence of solar wind driving and ionospheric dissipation the system is a three-degree-of-freedom Hamiltonian system. The large ion gyroradius conductance of the quasineutral sheet produces the energization of the central plasma sheet (CPS) while the unloading is triggered when the net geotail current or current density exceeds a critical value. For a steady southward IMF the model predicts an irregular sequence of substorms with a mean recurrence period of about 1 hr as in the Klimas *et al.* (1992) Faraday loop model. Here we use the new model as a nonlinear prediction filter on the Bargatze *et al.* (1985) database. Starting with physics calculations of the 13 physical parameters of the model we show that the average relative variance (ARV) is comparable to that obtained with data-based prediction filters. To obtain agreement between the predicted AL and the database AL it is essential to include the nonlinear increase of the ionospheric conductance with power deposited in the ionosphere.

AGU Indices: Magnetospheric Physics: (MS) 2740, 2788, 7839

1 Introduction

Developing a scientific understanding as well as obtaining predictive capability of substorm dynamics requires global modelling of the power flow from the solar wind through the magnetosphere to the ionosphere. The problem is many faceted with a long history but recent observations from the Geotail, Wind and Interball satellites bring into sharp focus the geometrical structure and the energetics of the driven magnetospheric-ionospheric system. Even

quantifying the solar wind input is a difficult aspect of the problem (Perrault and Akasofu, 1978). The dominant model at the present time is that during periods of southward IMF the solar wind driven dawn-to-dusk electric field E_y measured by $v_x^{\rm sw}B_s$, reduced by the reconnection efficiency $\beta_{\rm sw}$ (Hill, 1975), drives the geomagnetic tail plasma current until the system is sufficiently stressed to undergo an unloading event (Baker *et al.*, 1993). The precise location and cause of the unloading event remains unknown. The two leading candidates are the tearing of the thinned current sheet by the onset of the resistive MHD instability as seen in MHD simulations (Birn and Hesse, 1996; Ogino *et al.*, 1996), or the onset of a cross-field current driven microinstability producing a current diversion (Lui *et al.*, 1990). There is, however, no clear statistical correlation between either of these models and observations. Thus, there are other theories that argue either that the system is purely a driven system (Akasofu, 1980) or that the trigger for the onset of the expansion phase of the substorm lies in the condition of the solar wind (Lyons, 1996). Lyons argues that the trigger for substorms is in the IMF orientation rather than an internal magnetospheric instability. Such an IMF trigger appears compatible with the energy release mechanism described in Horton and Tajima (1988).

While global MHD simulations (e.g. Brecht *et al.*, 1982; Usadi *et al.*, 1993; Fedder and Lyon, 1995) provide useful coarse grain information on the solar wind-magnetospheric interactions, kinetic processes (Ashour-Abdalla *et al.*, 1994, Winglee and Steinolfson, 1993) are recognized to play a critical role in the energy conversions at the magnetopause and the quasineutral sheet. Here we extend the low-dimensional energy conserving model of Horton-Doxas (1996) to include the ionospheric coupling through the region 1 currents. The Horton-Doxas nonlinear dynamics model (hereafter the NLD model) includes the large ion gyroradius kinetic physics in the quasineutral sheet that converts $\mathbf{E}\times\mathbf{B}$-convection to thermal plasma energy through the chaotic conductivity [Horton and Tajima, 1990, 1991] and the finite parallel heat flux neglected in ideal MHD.

The large ion gyroradius conductivity gives a finite conductance Σ and nonadiabatic ion thermalization in the quasineutral sheet $\Delta Z = (\rho_i L)^{1/2}$ which vanishes in the MHD limit. The conduction was derived from theory and test particle simulations and contains the Lyons-Speiser (1982) energization mechanism for the transient ions as part of the ensemble average over the modified Harris sheet equilibrium. The kinetic loss rate of thermal energy is described by the parallel heat flux (the skewness of the ion velocity distribution) by a heat flux limit parameter and the mean parallel flow velocity associated with the MHD parallel flow kinetic energy, $K_\parallel(t)$. The Geotail particle data is currently being analyzed with respect to the parallel thermal flux (private communication Hoshino *et al.*, 1996).

The Horton-Doxas NLD model is closely related to the Klimas *et al.* (1992, 1994) Faraday loop model (FLM) which uses the "dripping faucet" analogue for the release of stored energy. In the NLD model the release of stored energy is triggered by the geotail current or current density exceeding a critical value I_c and the unloading rate is taken from the parallel ion thermal flux $q_\parallel(t)$ that occurs at the onset time $I = I_c$. Under a steady southward IMF the system undergoes a sequence of loading-unloading cycles with mean recurrence time of order 1 hour as reviewed in Klimas *et al.* (1996). Here we report the development and behavior

of a new extension of the model to include a self-consistent coupling to the ionosphere. The new model is a three degree of freedom Hamiltonian model in the limit of no driving and dissipation.

There are many works describing the onset condition for tearing modes (Terasawa, 1981, Birn and Hesse, 1996) and the cross-field current driven instabilities (Lui *et al.*, 1990). We do not dwell further on the details of the trigger in this work.

2 The Magnetospheric-Ionospheric Nonlinear Dynamics Model

Without repeating the derivation of the $d = 4$ geotail model in Horton-Doxas (1996) we describe the $d = 6$ model, and in particular the coupling of the region 1 current loop to the geotail current loop and the conductance of the ionosphere. The state space for the original model is given by $X^\alpha = [I, V, P, K_\parallel]$. The geotail system has 9 parameters $\{\mu\}_{i=1}^9$ based on the physical analysis of the MHD system with the kinetics of the large ion gyroradius quasineutral layer and the parallel ion thermal flux. The state space for the present model is $d = 6$ with the state vector

$$X^\alpha = [I, V, P, K_\parallel, I_1, V_I]. \tag{1}$$

The four additional physical parameters required for this extended model are (i) the mutual inductance M, (ii) the self-inductance $\mathcal{L}_1$, (iii) the capacitance C_1 and (iv) the conductance, Σ_I, of the ionosphere. The complete parameter list for the model is

$$\{\mu\} = [\beta_{\rm sw}, \mathcal{L}, C, \Sigma, \Omega_{\rm cps}, \tau_\parallel, u_0, I_0, \Delta I, M, \mathcal{L}_1, C_1, \Sigma_I]. \tag{2}$$

The closest comparable analog model is that of Klimas *et al.* (1994) that couples the earlier Faraday loop dripping faucet model (Klimas *et al.*, 1992) to the ionosphere by a linear second order filter for the AL index. The nonlinear dynamics part of the Klimas *et al.* (1994) model has the three-dimensional state space variables: (1) the average cross-tail electric field $E(t)$ corresponding here to $V(t)/L_y$, (2) the time varying magnetic flux $\phi(t)$ in the lobe corresponding here to $\mathcal{L}I(t)$ and (3) a dimensionless measure $\beta(t)$ of the plasma trapped in the lobe reversed magnetic field $P_0 = B_L^2/2\mu_0$ corresponding here to $P_0(t)$. The fourth equation of the Horton-Doxas system for the parallel streaming kinetic energy is replaced in the Klimas *et al.* model by a switching rule that dictates a strict linear in time rise or fall of the β-variable according to whether the magnetic flux $\phi(t)$ is below or above a critical value ϕ_c. Below ϕ_c the loading rate is $d\beta/dt = C_L\varepsilon_0(t)$ where $\varepsilon_0(t)$ is the scaled value of $V_{\rm sw}B_s$, and above ϕ_c the unloading rate is $d\beta/dt = -C_D\dot{\phi}(t_c)$ where $\dot{\phi} = d\phi/dt$ is taken at the most recent crossing of $\phi > \phi_c$. The variability of $\dot{\phi}$ according to the phase of the $\{E, \phi, \beta\}$ system gives rise to the chaos in this three-dimensional system. To connect this magnetotail model to a VB_s-AL database requires the time scale $\tau_0 \sim (\mathcal{L}C)^{1/2}$ choice from the dimensionless time τ of the model, the solar wind coupling efficiency $\beta_{\rm sw}$, the damping

ν, and three parameters of the Weimer-type linear, passive filter — rise time τ_r, decay time τ_d and coupling strength $C_0 = \delta(AL)/\delta E$. Thus, the equivalent Klimas *et al.* (1994) analog model requires 9 parameters $\{\beta_{\rm sw}, \tau_0, \nu, \phi_c, C_L, C_D, \tau_r, \tau_d, C_0\}$.

The lower dimensions of the state space and smaller parameter set is an advantage of the Klimas *et al.* model. The restriction of the model to a linear dynamics of $\beta(t)$ and the loss of the parallel mass flow prediction would appear to be a serious restriction in describing the state of the geotail. Perhaps the most serious difference in the two models, however, follows from the inability of the Klimas *et al.* model to describe the nonlinear dynamics of the ionospheric coupling. The ability of the present model to keep track of the various magnetospheric and ionospheric energy components throughout the evolution of a substorm is thought to be a significant advantage worth the cost of the higher dimensionality of the model. Clearly, an important future task is to compare the performance of the two models on the same database. Here, however, we concentrate on presenting the new six-dimensional NLD model.

2.1 Six-dimensional nonlinear dynamics equations

The $d = 6$ magnetotail-ionospheric nonlinear dynamics model is given by

$$\mathcal{L}\,\frac{dI}{dt} = V_{\rm sw}(t) - V + M\,\frac{dI_1}{dt} \tag{3}$$

$$C_{\rm cps}\,\frac{dV}{dt} = I - I_1 - I_{ps} - \Sigma V \tag{4}$$

$$\tfrac{3}{2}\,\frac{dP}{dt} = \Sigma\,\frac{V^2}{\Omega_{\rm cps}} - u_0\,K_\parallel^{1/2}\Theta(I - I_c)P \tag{5}$$

$$\frac{dK_\parallel}{dt} = I_{ps}V - \frac{K_\parallel}{\tau_\parallel} \tag{6}$$

$$\mathcal{L}_I\,\frac{dI_1}{dt} = V - V_I + M\,\frac{dI}{dt} \tag{7}$$

$$C_I\,\frac{dV_I}{dt} = I_1 - \Sigma_I V_I \tag{8}$$

Here the pressure gradient driven current is given by $I_{ps}(t) = \alpha P^{1/2}(t)$ as derived from $\mathbf{j} \times \mathbf{B} = \nabla P$ force balance and Amperé's law. The solar wind driving voltage in Eq. (3) is $V_{\rm sw} = \beta_{\rm sw} v_x^{\rm sw} B_s^{\rm IMF} L_y$. The coefficient $\beta_{\rm sw}$ reflects the efficiency with which the solar wind electromotive force is translated into a cross-tail potential drop. For reference the value of $\beta_{\rm sw}$ taken following Goertz *et al.* (1993) is $\beta_{\rm sw} = 0.1$. The solar wind voltage $V_{\rm sw}(t)$ is the input time series from the nonlinear driven-dissipative system.

The form of the Eqs. (3)–(8) can be understood as the variational equations for the action S for the electromagnetic fields when the current paths are fixed and the current-

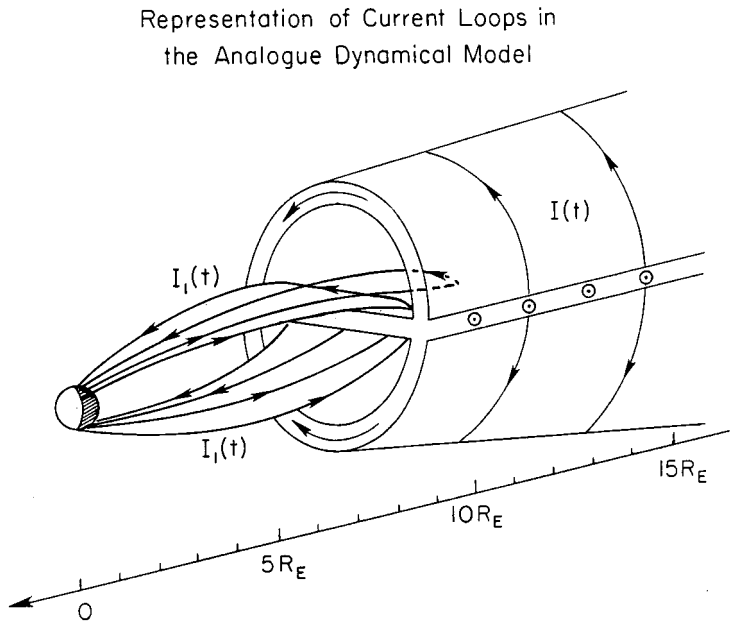

Figure 1: Representation of the topology of the two current systems $I_1(t)$ and $I(t)$ used in the nonlinear dynamical model. The current systems are distributed and the lines for the current loops are purely schematic for the distributed plasma currents.

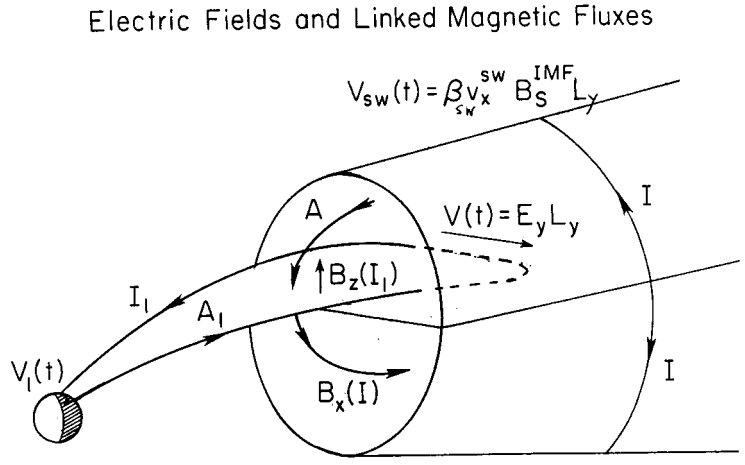

Figure 2: Representation of the three voltages $V_{\rm sw}(t), V(t)$ and $V_I(t)$ used in the NLD model. The Faraday loop integral around the I_1-current path determines the $V_I(t) - V(t)$ voltage difference in terms of the self-induction $\mathcal{L}_1$ and the mutual inductance M from the $B_z(I_1)$ and $B_x(I)$ magnetic fields as shown.

voltage pairs (I, V, I_1, V_I) are the variational parameters on the specified current paths. The arrangement of the linked current systems and the definitions of the voltages is shown in Fig. 1. The associated magnetic fields and the coupling of the flux from the magnetotail current through the region 1 current loop is shown in Fig. 2. The variational description for the electromagnetic field equations is given by the Lagrangian density $B^2/2\mu_0 - \epsilon E^2/2$ with the $\mathbf{E}$ and $\mathbf{B}$ fields expressed through the vector potential $\mathbf{A}$ and the scalar potential $\phi(\mathbf{x}, t)$. Maxwell's equations follow from the functional variation of

$$S = \int d^3x dt \left(\frac{\mathbf{B}^2}{2\mu_0} - \tfrac{1}{2}\,\epsilon(\mathbf{x})\mathbf{E}^2 \right) \tag{9}$$

with respect to $\mathbf{A}$ and ϕ. Once the current paths are specified the magnetic energy term W_B in Eq. (9) reduces to

$$W_B = \int \frac{B^2}{2\mu_0} d^3x = \tfrac{1}{2}\Sigma_i \mathcal{L}_i I_i^2 + \Sigma_{i,j} M_{ij} I_i I_j \tag{10}$$

where $\mathcal{L}_i$ and $M_{i,j}$ are the standard well-defined path integrals for the self and mutual inductances. The definitions for the capacitances follow from reducing the electric field energy

$$W_E = \tfrac{1}{2} \int \epsilon_\perp(x) E_\perp^2 d^3x = \tfrac{1}{2}\, C_{\rm cps} V^2 + \tfrac{1}{2}\, C_1 V_1^2 \tag{11}$$

where $\epsilon_\perp = \rho_m(\mathbf{x})/B^2(\mathbf{x})$ accounts for the polarization of the plasma. Thus, the electric field energy, $W_E = \frac{1}{2}\int \rho_m V_E^2 d^3x$, is the $\mathbf{E} \times \mathbf{B}$ kinetic energy from plasma convection. More details on the derivation of Eqs. (3)–(8) are given in Horton-Doxas (1996).

From Fig. 2 it is clear that growth of the magnetotail current $I(t)$ produces a negative ΔB_z in the Earthward edge of the central plasma current sheet that links the I_1-current loop with $M = (\mu_0 L_{xI} L_{yI}/L_x)\ell n(L_{xI}/L_{yI}) \sim 10\,\mathrm{H}$ where L_{xI} and L_x are the lengths of the region 1 and geotail current loops and L_{yI} is the dawn-dusk dimension of the region 1 current loop in the central plasma sheet. The Faraday loop integral around the region 1 current circuit gives Eq. (7) where we see that during the growth phase of the magnetotail current $MdI/dt > 0$ there is an inductive electric field driving up the region 1 current. The conservation of charge for the quasineutral system follows from the volume integral of $\nabla \cdot \mathbf{j} = 0$ yielding Eq. (8) which states that the total region current I_1 equals the sum of the plasma polarization current from $\mathbf{j}_{p1} = (\rho_m/B^2)(d\mathbf{E}_1/dt)$ and the ionospheric current from the Pedersen conductivity Σ_I. This conductivity arising from the neutral collisions is the only true dissipation in the system. Due to this ionospheric dissipation the quiet time magnetosphere (with $v_x^{\rm sw} B_s^{\rm IMF} = 0$) has an ambient 30–35 kV potential for $V = V_{\rm sw}$ in Eq. (3) (Reiff *et al.*, 1981). Thus, the empirical solar wind driven voltage has the base level $V_0 \simeq 30\,\mathrm{kV}$ with $V_{\rm sw} = V_0 + \beta_{\rm sw} v_x^{\rm sw} B_s^{\rm IMF} L_y$ in Eq. (3). For the steady state this gives $I_1 = \Sigma_I V_0$ which for $\Sigma_I = 3\,\mathrm{mho}$ gives the ambient $I_1 \simeq 10^5 A$. The capacitance C_1 is difficult to calculate: currently we are using $C_1 = 10^3\ F$ giving the RC_1—decay time for the quiet-time I_1 current loop of $\tau = C_1/\Sigma_I \cong 5$ min. A more detailed description including pressure gradient sources in the region 1 currents will be developed following Yang *et al.* (1994) in the future.

2.2 Energy Conservation

The NLD model is based on the six energy components essential in describing the disturbed times of the magnetotail-ionospheric system. These components are also the key energy components of the resistive MHD dynamics of reconnection. They are: (1) lobe magnetic field energy: $\int_{\rm lobe} \frac{B^2}{2\mu_0}\, d^3x = \frac{1}{2}\,\mathcal{L}I^2$ ($\sim 8\times 10^{15}$ J); (2) $\mathbf{E}\times\mathbf{B}$ kinetic energy: $\int_{\rm cps} \frac{1}{2}\,\rho_m u_\perp^2 d^3x = \frac{1}{2}\,C_{\rm cps}V^2$ ($\sim 4\times 10^{13}$ J); (3) parallel kinetic energy: $\int_{\rm cps+psbl} \frac{1}{2}\,\rho_m u_\parallel^2 d^3x = K_\parallel$ ($\sim 3\times 10^{14}$ J); (4) central plasma sheet thermal energy: $U_p = \int_{\rm cps}\left(P_\perp + \frac{1}{2}\,P_\parallel\right) d^3x \cong \frac{3}{2}\,P\Omega_{\rm cps}$ ($\sim 3\times 10^{14}$ J); (5) ionospheric $\mathbf{E}\times\mathbf{B}$ kinetic energy: $W_i = \frac{1}{2}\,C_I V_I^2$ ($\sim 3\times 10^{12}$ J); and (6) ionospheric magnetic energy: $\frac{1}{2}\,\mathcal{L}_I I_1^2$ ($\sim 10^{12}$ J) associated with the region 1 current. There is also an interaction energy component $W_{gt,i} = -MII_1$ from the linkage of the lobe magnetic flux from I through the region 1 current loop as indicated by Fig. 2.

The total energy W is the sum of these components

$$W = \tfrac{1}{2}\,\mathcal{L}I^2 + \tfrac{1}{2}\,\mathcal{L}_I I_1^2 - MII_1 + \tfrac{1}{2}\,C_{\rm cps}V^2 + \tfrac{1}{2}\,C_I V_I^2 + \tfrac{3}{2}\,P\Omega_{\rm cps} + K_\parallel. \tag{12}$$

The dynamical Eqs. (3)–(8) give the rate of change of the energy

$$\frac{dW}{dt} = IV_{\rm sw} - \tfrac{3}{2}\,\frac{P\Omega_{\rm cps}}{\tau_E(I,K_\parallel)} - \frac{K_\parallel}{\tau_\parallel} - \Sigma_I V_I^2 \tag{13}$$

Here $\tau_E(I,K_\parallel)$ is the confinement time for the thermal plasma energy given by

$$\frac{1}{\tau_E(I,K_\parallel)} = \frac{2u_0}{3}\,K_\parallel^{1/2}\Theta(I-I_c)$$

where u_0 is a constant (Luciani *et al.*, 1983) such that $\tau_E \sim L_x/\overline{v}_\parallel$ in the $I > I_c$ unloading state. From the derivation of Eq. (5) the loss rate P/τ_E accounts for the thermal flux leaving the central plasma sheet volume $\Omega_{\rm cps}$ through Earthward and tailward fluxes (Horton and Doxas, 1996).

In the dissipationless limit and in the absence of the solar wind driving the energy W is conserved. The eigenmodes of the $W=$ const system are discussed in Appendix A. Now we discuss the energy transfer from the $\mathbf{E}\times\mathbf{B}$ flows to the thermal plasma energy.

The value of the plasma sheet conductance is calculated by Horton and Tajima (1990, 1991a, b) to be

$$\Sigma = \sigma_0 \frac{nq}{|B_z|}\left(\frac{\rho_i}{L_z}\right)^{1/2}\left(\frac{L_xL_z}{L_y}\right). \tag{14}$$

with $\sigma_0 = 0.1$. This may be compared to an estimate from the finite Larmor radius (FLR) two-component fluid theory (e.g. Braginskii, 1965), which gives a momentum stress tensor conductance of $(nq/B_z)(\rho_i/L_z)(L_xL_z/L_y)$. Thus the effect of the large-ion-orbits in the quasineutral layer, that are outside the domain of validity of FLR-MHD theory, is to change the exponent on the ρ_i/L_z dependence of the Hall-type conductance.

In the absence of driving and coupling to the ionosphere and ring current the system has the energy integral in Eq. (12). The energy integral in Eq. (12) corresponds directly to the MHD energy integral containing the total magnetic energy W_B, the total perpendicular $\mathbf{E}\times\mathbf{B}$ flow energy K_E, the parallel kinetic energy $K_\parallel$ and the thermal energy U_p.

2.3 Ionospheric Conductance

Initial studies of the NLD model used a constant conductance of a few mhos for the ionospheric response. The resulting values of the I_1 current were too low in magnitude and too slowly varying in time to account for the AL index. Realizing that the power deposited into the ionosphere is large ($\geq 10^9$ W) we turned to using a nonlinear conductance $\Sigma(P_{\rm ion})$ that increases with the joule heating $P_{\rm ion} = I_1 V_I$ deposited by the westward electrojet current. Thus, we adopt the Robinson *et al.* (1988) formula for the power flux Φ_E dependence of the Pedersen conductivity which is proportional to $\Phi_E^{1/2}$. The Robinson *et al.* (1988) conductivity is $\Sigma = \Sigma_\Phi \Phi_E^{1/2} \sim$ few mhos for $\Phi_E = 1\,{\rm erg/cm^2 \cdot s} = 10^{-3}\,{\rm W/m^2}$. Thus, we use for the ionospheric conductance model

$$\Sigma_I = 1.0 + 2.0 \times 10^{-4} (I_1 V_I)^{1/2} \tag{15}$$

giving the base level of 1 mho and the increase to $1 + 2(10)^{1/2} = 7.3$ mho for an ionosphere power deposition of $I_1 V_I = 10^9$ W. In terms of power per unit area Φ_E the coefficient in Eq. (15) is equivalent to the Robinson *et al.* (1988) value for an auroral arc region of size $\Delta\theta$ a few degrees at $\theta = 70^\circ$ latitude with a longitudinal length of $\ell_\phi = 1800$ km ($\Delta\phi = 50^\circ$) receiving $P_{\rm ion} = 1$ GW of joule heating. Instead of one long auroral arc the system may have multiple shorter arcs with the same area $\sim 10^{12}\,{\rm m^2}$.

The conductance formula (15) brings the model into agreement with the profile of conductance taken from the Hilat satellite passage over Sondre Stromfjord shown in Fig. 5 of Robinson *et al.* (1988). In that figure the conductances rises from ≈ 1 mho to a broad peak from 4 to 8 mhos within the latitude range $\theta = 69^\circ$ to 74°.

An obvious future extension of the model is to add another (second) trigger function such that parallel potential drops producing precipitating electron fluxes are triggered when the upward region 1 current density $j_\parallel > j_{\rm crit} \sim 10^{-6}\,{\rm A/m^2}$. Adding the physics of the parallel accelerator zones would allow the model to calculate the precipitating electron energy flux while addressing the observations for the correlation of such potentials with substorms as reported in the DE-1/DE-2 conjunction studies of Reiff *et al.* (1981). The nonlinear increase of the ionospheric conductance by $(I_1 V_I)^{1/2}$ in Eq. (15) is a model for the ionization produced by the precipitating electrons. A more complete model for this process should be included in a future development.

The nonlinear increase of the conductance with $P_{\rm ion}$ has the effect of making a sharp increase of I_1 that brings the model into much better agreement with the AL data. The ionospheric response time $\tau_1 = C_1/\Sigma_I$ is now a strong function of the phase and the strength of the substorm.

3 Behavior of the NLD Model

Figure 3 shows the performance of the model as a nonlinear prediction filter using only the VB_s-input for interval 20 of the Bargatze *et al.* (1985) data. The six panels from top to bottom show (1) the $V_{\rm sw}$ input voltage, (2) the geotail $V(t)$ and ionospheric $V_I(t)$ voltages

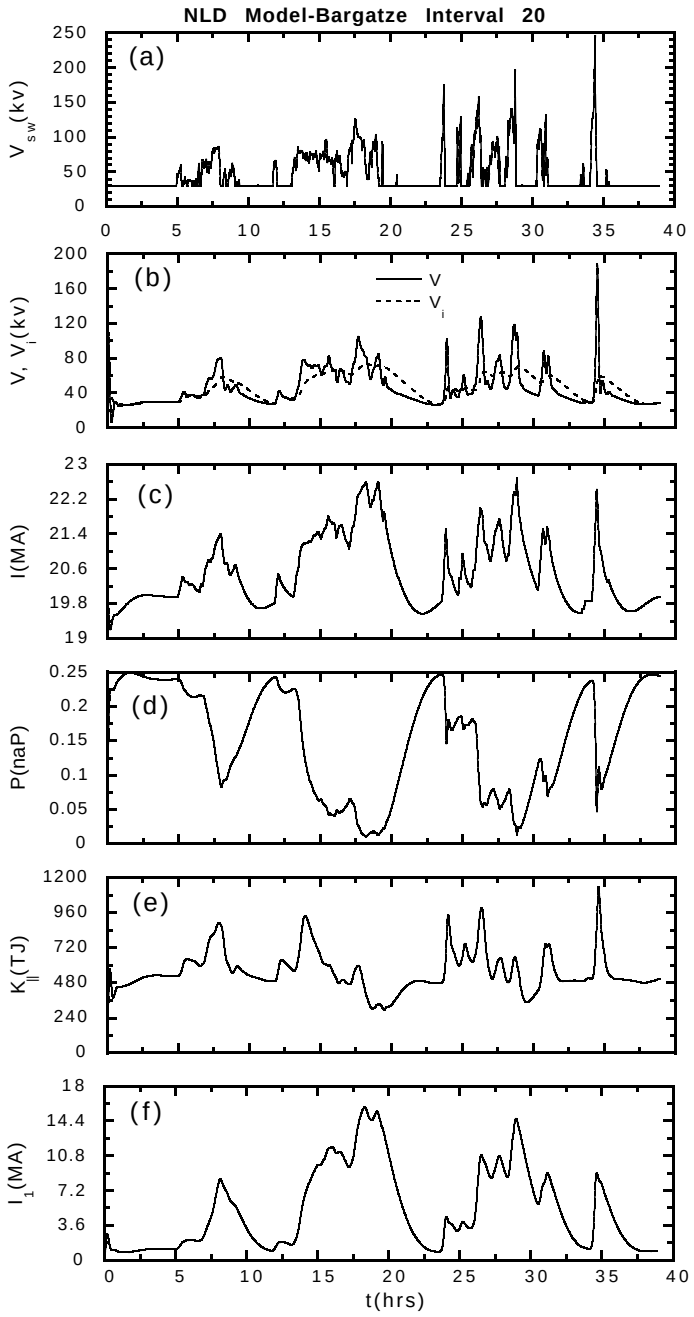

Figure 3: Prediction of the NLD model using the Bargatze interval 20 for the input and the target AL time series. From the top, the six panels show (a) the $V_{\rm sw}$ input voltage, (b) the geotail $V(t)$ and ionospheric $V_I(t)$ voltages which are equal in the steady state, (c) the current $I(t)$ in the magnetotail, (d) the central plasma sheet pressure $P(t)$, (e) the total parallel kinetic energy $K_{\|}(t)$ in the mass flows and (f) the region 1 current I_1 that closes as a westward electrojet in the ionosphere producing the predicted AL index.

which are equal in the steady state, (3) the current $I(t)$ in the magnetotail current (4) the average central plasma sheet pressure $P(t)$, (5) the net kinetic energy $K_{\|}(t)$ in parallel mass flows and (6) the current $I_1(t)$ in the westward electrojet formed by the ionospheric closure of the nightside region 1 current loop.

In Fig. 4 we compare the model $AL(t)$ index computed from $I_1(t)$ and the $AL(t)$ for this 40-hour interval from Bargatze *et al.* (1985). For this interval there are three well separated peaks of $\sim 200\,\mathrm{nT}$ and one four-hour period (16-20 hr) with multiple intensification peaks two of which exceed 500 nT. For the standard comparison of the model AL to the data, we define the average relative variance (ARV) by

$$\mathrm{ARV} = \frac{\sum_{j=1}^{M} \left(O_j - \widehat{O}_j\right)^2}{\sum_{j=1}^{M} \left(O_j - \overline{O}\right)^2}$$

where O = measured output here $- AL(t)$, $\widehat{O}$ = predicted output taken as $\alpha I_1(t)$, and $\overline{O}$ = mean value of the output data.

The overall 40 hr average-relative-variance ARV for the model is 0.33 while for the subintervals containing the $\sim 200\,\mathrm{nT}$ substorm peaks, broken out in Fig. 4b and c, the ARV's are 0.23 for the period [5–12 hr] and 0.24 for the period (32–39 hr). Qualitatively, the best prediction is for the last substorm (32–40 hr) where only the $AL(t)$ fine structure is missing in Fig. 4c. In the first-subinterval (5–12 hr), while the ARV is equally low, there is a qualitative problem with the growth phase continuing too long (by $\sim 20\,\mathrm{min}$) and the rate of increase of $-AL$ in the expansion phase being too slow.

3.1 Parameter Values for the NLD Model

The values of the parameters used in the example given here were set as follows. First the values are calculated from the geometrical and plasma parameters known from the physics of the geotail-ionosphere system. Then simple one-dimensional parameter scans for the variation of the ARV with respect to the value of $\mathcal{L}, \Sigma, C$ and β_{sw} were carried out. The results of the scans are shown in Fig. 5 and the four values were adjusted accordingly. An encouraging fact was that modest changes in the parameter values derived from the physics were required to be located at the minimum ARV in each of these single-parameter scans. A systematic search for minima of ARV $\{\mu\}$ will give a lower ARV model for this interval. While such minimization work is underway, we note that the spirit of the physics-based model is to rely heavily on approximate calculations of the parameters of the model. By using global magnetospheric models such as the Tsyganenko (1989) model detailed calculations for the system parameters can be performed. Clearly, some parameter adjustments minimizing the ARV are called for since the accuracy of the calculations for the $\{\mu\}$ parameters is limited. Numerous software packages are available that can be used to find minima of ARV $\{\mu\}$. The values used in the present report are given in Table 1. Here we discuss a few features of the

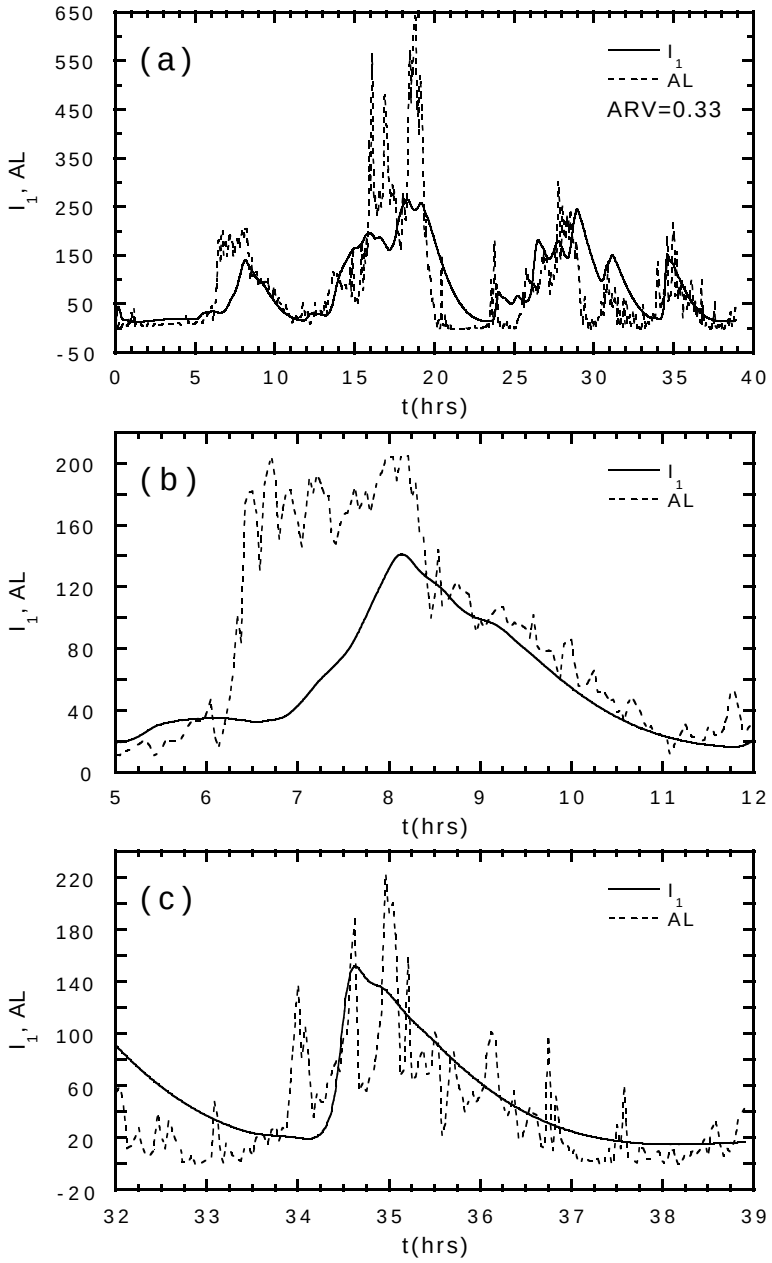

Figure 4: Comparison of the predicted (solid line) from the Bargatze database. Frame (a) shows the entire 39 hr interval with an ARV of 0.33 and frames (b) and (c) shows the details of the predicted and target data for the two isolated substorms in the subintervals (b) [5, 12 hr] with ARV = 0.22 and (b) [32, 39 hr] with ARV = 0.24.

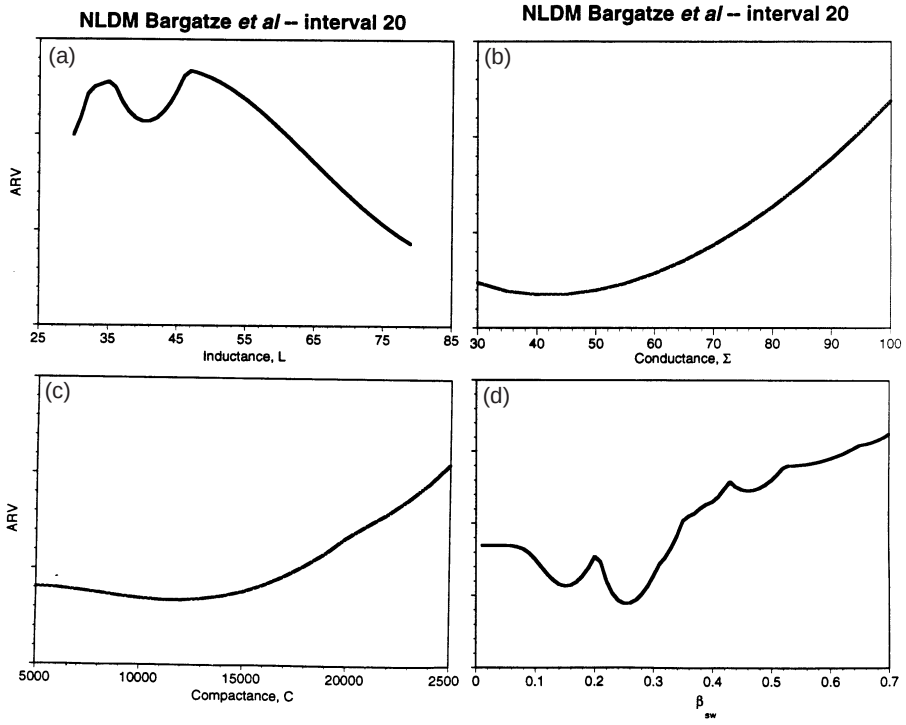

Figure 5: One-dimensional parameter scans for the average relative variance (ARV). Variations with (a) the lobe inductance $\mathcal{L}$, (b) the central plasma sheet conductance Σ, (c) the central plasma sheet capacitance C, and (d) the solar wind coupling efficiency $\beta_{\rm sw}$.

system that follow from this parameter set. The global Alfvén period is $T_{gt} = 2\pi(\mathcal{L}C)^{1/2} = 1.2$ hr and the ionosphere coupling Alfvén period is $T_A = 2\pi(\mathcal{L}_1 C_1)^{1/2} = 11.5$ min. For the mean geotail current of $I = 20\,\mathrm{MA}$ the geotail magnetic energy $W_B = 8 \times 10^{15}\,\mathrm{J}$ while the central plasma sheet thermal energy $U_p = 9 \times 10^{14}\,\mathrm{J}$. The ambient or base-line value of the inductive coupling magnetic energy is $W_{gt,i} = -MII_1 = -10^{14}\,\mathrm{J}$. The ionosphere current loop has the baseline value of $I_1 \sim 4 \times 10^5\,\mathrm{A}$ and associated magnetic energy of $W_i = 10^{12}\,\mathrm{J}$, but large increases of the ionospheric energy W_i occur with peaks reaching $1 - 3 \times 10^{14}\,\mathrm{J}$ for periods ≤ 1 hr during the substorms.

In the absence of the ionosphere conductance ($\Sigma_I = 0$) and with the parallel thermal flux losses taken to zero the system conserves energy with $E_{\rm total} \sim 10^{16}\,\mathrm{J}$. Opening the system to the solar wind driving and the ionospheric dissipation from joule heating gives an intermittent power transfer through the system which we now discuss.

Figure 6 shows the powers transferred through the system. First the driving input power is $P_{\rm in}(t) = I\beta_{\rm sw}\, E_y^{\rm sw} L_y$ with a base level of 0.6 TW and spiky peaks reaching 3 to 5 TW as shown by the solid line. The power P_p is that transferred to the central plasma sheet pressure (lowest dashed curve) and $P_{\rm par}$ is the power transferred to the parallel kinetic energy $K_\parallel$ (the intermediate short-long dashed curve). The ionospheric power transfer $P_{\rm ion}(t)$ is a

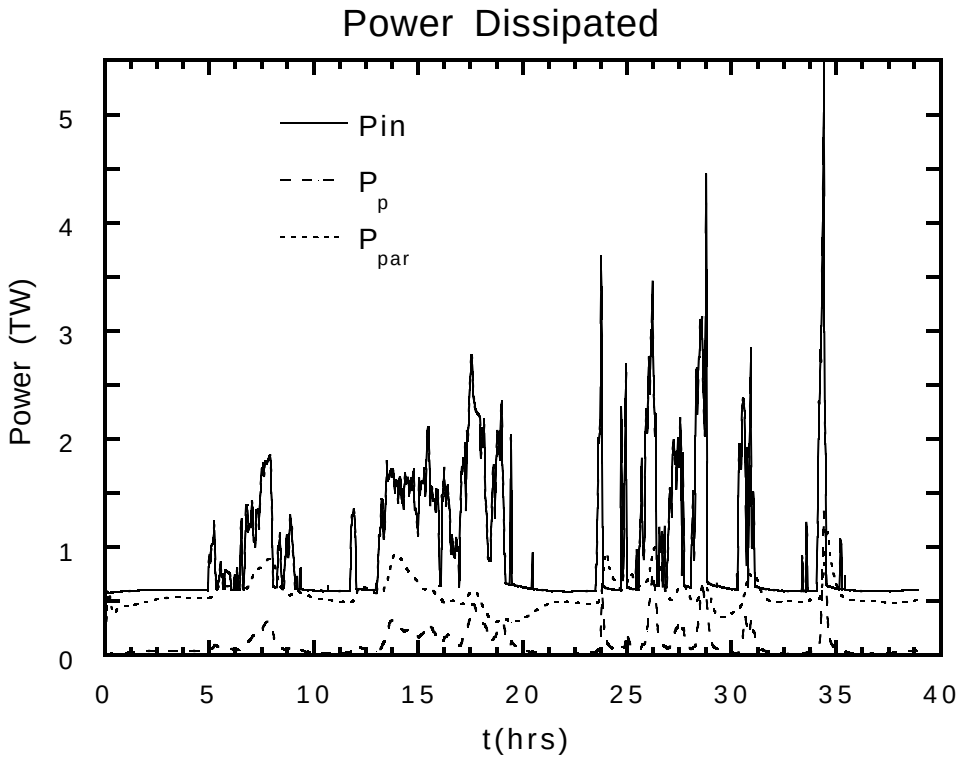

Figure 6: The power transfers that occur during interval 20 shown in Fig. 4. In decreasing magnitude is the total power input $P_{\rm in}$ (solid line), the power to the parallel ion mass flows (short dashed line) and the power to the plasma thermal energy (long-short dashed curve).

few percent of the input power and did not show well on the scale of Fig. 6. Thus, the fraction of the solar wind input power transferred to ionospheric joule dissipation $P_{\rm ion}(t) = I_1 V_I$ is shown in Fig. 7. This signal is "spiky" in structure giving the qualitative picture of an intermittent heating of the ionosphere. It was the study of this figure that lead the authors to the conclusion that it is important to include the nonlinear response of the ionospheric conductivity to the deposited power. The Robinson *et al.* (1988) conductance formula is used for this purpose and resulted in a marked improvement in the quality of the AL prediction. Analysis shows that model (15) leads to an amplification of the stochastic components of the solar wind input for $V_{\rm sw}$ greater than a critical value of order 60–80 kV.

3.2 Response Times of the NLD System

The multiple time scales of the underlying linear dynamics are determined analytically in the Appendices. In Appendix A the high and low oscillation frequencies of the coupled magnetotail and region 1 current loops are determined for the closed, dissipationless, Hamiltonian limit of the system. In Appendix B the dissipative ionospheric response function is derived and shown to reduce to the Weimer model used by Klimas *et al.* (1994) in the limit where the

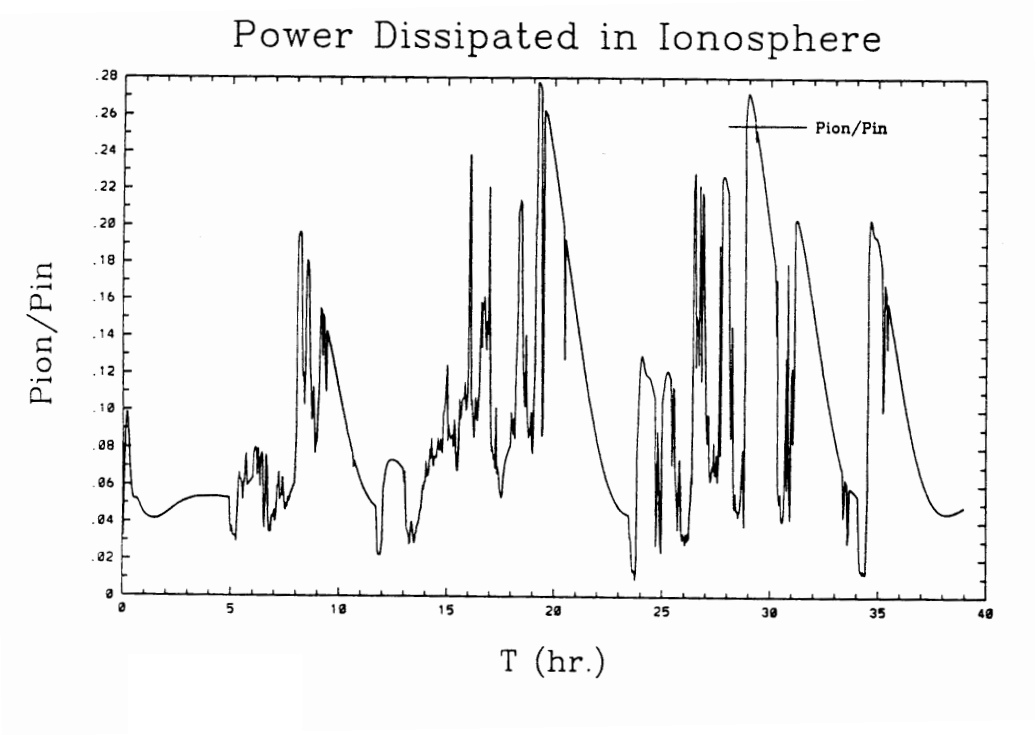

Figure 7: The power dissipated in the ionosphere $P_{\rm ion}$ as a fraction of the total input power.

feedback from the ionosphere to magnetosphere is neglected and the ionospheric dynamics is linear. The operational regime of the NLD system for the Bargatze database, however, is nonlinear and contains complicated combinations of the linear time scales and the nonlinear loading-unloading cycling period reported in Horton and Doxas (1996) and reviewed in Sec. III of Klimas *et al.* (1996) on the status of *analogue models*. To address the question of how the NLD model represents the 20–30 min time delay observed in substorm data we have applied impulsive inputs of $V_{\rm sw} = V_p\delta(t - t_p)$ to the ambient steady state where $V_{\rm sw} = 30\,{\rm kV}$ with the reference system parameters used in Figs. 4–7. The response of the I_1 current to the impulse is $h(\tau) = \Delta I_1(t - t_p)/V_p$, the generalization of the linear response function to this system, was obtained for a sequence of pulse strengths $V_p = \{60, 90, 120, ..., 200\,{\rm kV}\}$. The results for $V_p = 60\,{\rm kV}$ is shown in Fig. 8 and is typical of the $V_p \lesssim 120\,{\rm kV}$ result. For higher values of V_p the recovery time is longer while the rise time $\tau_r \sim C_1/\Sigma_I$ is shorter due to the nonlinear increase of the ionospheric conductance.

From Fig. 8 we see that the maximum of the response occurs at the delay $\tau_D = t_1({\rm max}\ I_1) - t_p \simeq 21.6\,{\rm min}$. Parameter variations of the model show that for the parameter range of interest the delay time $\tau_D \equiv t({\rm max}\ I_1) - t_p$ varies only weakly. The strongest variation is with the lobe inductance $\mathcal{L}$ and central sheet capacitance C and can be approximated by $\tau_D = \tau_0(\mathcal{L}/\mathcal{L}_0)^x(C/C_0)^y$ where we find that $x \simeq 0.7$ and $y \simeq 0.3$.

The long period ($\gtrsim 60\,{\rm min}$) dynamics in times of southward IMF is associated with the bifurcation that occurs when the plasma sheet current exceeds I_c. Formulas for the

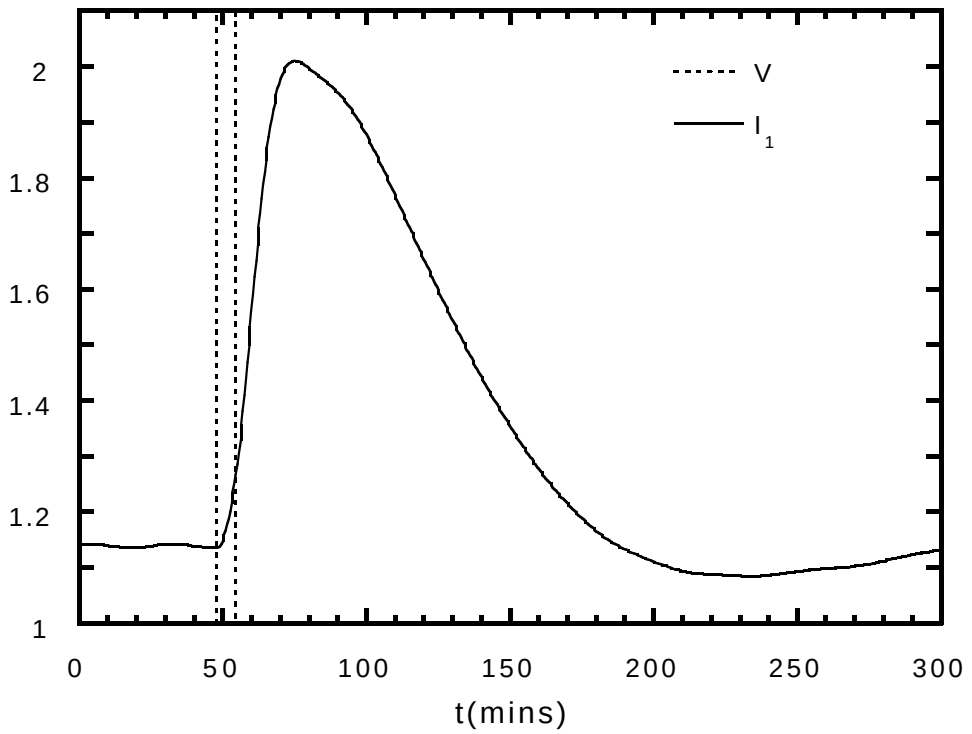

Figure 8: The nonlinear response $I_1(t)$ from the model to an impulsive input $V_{\rm sw}(t) = 60\,{\rm kV}\delta(t - t_p)$ shown by the vertical dashed lines at $t_p \simeq 49$–53 min. The delay time $\tau_D \simeq 22\,{\rm min}$ to the maximum response in the westward electrojet current is a persistent feature of the model.

bifurcation condition, the limit cycle frequency and the numerical study of the (distribution of) recurrence times are given in Horton and Doxas (1996) and compared by Klimas *et al.* (1996) with the recurrence times reported in Klimas *et al.* (1994). Horton and Doxas (1996) show that the recurrence time shortens as the strength of the solar wind drive increases. Above a critical driver the response merges into the short 20 min response.

A recent re-examination by Smith and Horton (1997) of the Bargatze *et al.* (1985) time series sorted by average AL levels into 34 intervals shows clearly the dependence of the first delay time $\tau_{D,1}$ and the increasing strength of the first response $h(\tau_{D,1}) \sim a_1$ with the strength of the substorm. The trends in the nonlinear response function for the present model appear consistent with those of the linear Wiener filter derived for the Bargatze data. Clearly, an important future project is to quantify the comparison of the $\overline{\rm AL}$ sorted sequence of linear prediction filters with the nonlinear analogue model presented here.

Of the two components of the region 1 current system (Iijima and Potemra, 1978) the nightside currents and the dayside currents: the NDL model only includes the nightside DP-1 or substorm wedge current system. The dayside current region 1 loop gives a faster response on the time scale of minutes and generally an eastward ionospheric electroject signature. For stronger substorms the dayside region 1 current signature on the ground-based

magnetometers is on the AU index. Thus, we argue that the 20 min response on the AL index is a nightside feature of the magnetospheric-ionospheric system. A qualitative understanding of how the NLD model gives a strong, fast night-side response follows from the importance of the inductive electromotive force MdI/dt driving the I_1 current. Consider from Eqs. (3)–(8) the effect of a sudden increase $\Delta V_{\rm sw}$ in the solar wind driving voltage as in Fig. 8. The direct linear growth of I_1 arises from MdI/dt with $\Delta I_1 \propto (M\Delta V_{\rm sw}/\mathcal{L}\mathcal{L}_1)t$. Without the mutually linked magnetic flux ($M = 0$) the region 1 would increase as $\Delta I_1 \propto (\Delta V_{\rm sw}/C_{\rm cps}\mathcal{L}\mathcal{L}_1)(t^3/3)$.

In MHD simulations where the inner edge of the central plasma sheet moves inward and often there is the growth of a plasmoid, the flux linkage becomes even stronger. Thus, the strong direct drive of the nightside region 1 (DP-1) current system is an important feature of the magnetosphere-ionosphere model for the expansion phase. For the recovery phase the model proceeds too slowly compared with the empirical filter models. Whether further tuning of the parameters in the present model can shorten the recovery time is still under investigation. There are two areas that require further consideration. The nonlinear part of the conductivity may need a decay rate equation providing a faster return to the presubstorm conductivity. This decay of the enhanced conductivity level will speed up the recovery phase. The model may be expanded to include a stronger tailward ejection of plasma as in a plasmoid ejection. The plasmoid ejection modeling is within the scope of the theory developed in Horton and Doxas (1996). The model is energy conserving taking into account the flow of energy into and out of the volume $\Omega_{\rm cps}$ defining the dominant plasma energy containing part of the geomagnetic tail.

The DP-2 current system (Nishida, 1968) is a large space scale–long time scale ($\gtrsim 1\,$hr) current system approximately independent of the westward electrojet. The equivalent ionosphere current system is the sum of an eastward monopolar zonal flow and a dipole vortex. The present model would need to be expanded to incorporate the dayside region 1 current loop to address the AU index and the coupling to the DP-2 current system.

4 Conclusions

A nonlinear dynamics model of the coupling between the geotail and the ionosphere by the region 1 current leads to a nonlinear prediction filter for geomagnetic activity. The couplings and parameters of the dynamics in the $d = 6$ dimensional state space are derived from the known geometrical structure of the nightside magnetosphere as has been brought into sharp focus by the GEOTAIL and INTERBALL data reported at the 1996 Chapman Conference. Taking into account the global MHD constraints and the local kinetic physics in the quasineutral layer leads to the specification of the 13-parameter model. The new model is an extension of the earlier lower dimensional nonlinear dynamics models of Klimas *et al.* (1992, 1994) and Horton and Doxas (1996).

Viewed as a prediction filter the NLD model is a hybrid between an ARMA filter and a neutral network (NN). Writing the six ode's in finite difference form with a substantial time step shows the relation to the ARMA system while the nonlinear switch for the unloading of the central plasma sheet pressure plays the role of the switch-on function in the NN system.

In a NN the input signals are summed according to weights from the preceding layer. Here the switch is triggered by the most recent value of the geotail current or current density and uses the values of the pressure and the parallel kinetic energy to determine the response to the system going critical. The model can be tailored to specific current disruption physics such as the near-Earth neutral line from tearing modes or the cross-field current instabilities (Lui *et al.*, 1990). Once more experience with this dynamical system is obtained, the NLD model may provide a method to discriminate between various microphysics mechanisms in their degree of success in correlating with substorm databases.

An important advantage of the NLD model is that energy conservation guarantees a bound on the division of the solar wind input power into the various major energy components. Charge conservation is also satisfied by the Kirchhoff structure of the current systems. The structure of the dynamical equations is derived from the variational form of the electromagnetic field Lagrangian density. Most microphysics calculations suffer from the lack of an external macroscale driving-coupling dynamics, and this model provides such an external driver correlated with the global state of the magnetosphere.

The performance of the system is tested by choosing a Bargatze *et al.* (1985) interval of intermediate level. The interval 20 of intermediate level of activity was chosen for the comparison. First the values of four key solar wind-geotail parameters were varied about the values derived from the physics calculations. A standard error measure called the average relative variance (ARV) is shown to have minima close to the physics derived values. In Fig. 3 and 4 we show the predictions of the NLD model from the $v_x^{\rm sw} B_s$ input for the model parameter given in Table 1. The other thirty-three intervals have been run through the NLD model with the ARV's ranging from 0.29 (interval 34) to relatively large values ($\lesssim 0.6$) for the first several intervals at low average geomagnetic activity. The low activity level intervals also show the poorest ARV values in the modeling with the linear Weiner filters (Smith and Horton, 1997). The low coherence of the structures at low activity levels appears to be a problem for prediction filters in general.

In our view the model performs well. The closest competitive model is the neural net forecasting work of Hernandez *et al.* (1993), which shows the results for interval 21 of the Bargatze database. Two architectures were reported: (1) the state space reconstruction which uses time lagged AL values as input and (2) the nonlinear prediction filter which uses only the $v_x^{\rm sw} B_s$ as input. As one expects the state space reconstruction gives the lowest ARV $= 0.25$ compared to the ARMA model with ARV $= 0.28$ both using a lag time of 15 min. In general, the AL is not available in real time, and the model we present here is equivalent to the nonlinear prediction filter NN where the performance was considerably degraded (ARV $= 0.46$) with respect to the performance of the system using the state space reconstruction architecture. While there are reasons to suspect that the NN performance for the nonlinear prediction filter could have been improved, we see that the basic physics model presented here already has a lower ARV $= 0.33$ using only the $v_x^{\rm sw} B_s$ input. The nonlinear dynamics model has many fewer parameters (13 compared to over 100 weights for the NN) and presumably will, when fully implemented, take into account the nonlinear variations, such as that in the ionospheric conductance, that occur over a wide range of physical parameters.

A linear prediction filter given by Blanchard and McPherron (1993, 1995) will also be compared with the NLD model. Presently, that Blanchard and McPherron model has been applied to isolated substorms in another database. Currently, we are reproducing their findings on the isolated substorms. Smith and Horton (1997) have applied the 5-parameter linear bi-modal model to the standard multiple substorm database of Bargatze *et al.* (1985) finding results comparable with those derived here from basic principles.

Thus, while much research on nonlinear prediction filters remains to be done as stated in the Klimas *et al.* (1996) review article, we conclude that a strong case can be made for low-dimensional physics models as an alternative to signal processing prediction filters trained with databases. There is clearly room for both methods of forecasting and by comparing the strengths and weaknesses of the complementary methods we may faster arrive at a reliable space weather forecasting system.

Acknowledgments

We wish to acknowledge useful conversations with A. Klimas, R. Wolf, and D. Winningham. The authors thank Jinlong Wu for performing the simulations and emphasizing the importance of the nonlinear ionospheric conductance. The work was supported by the NASA Grant NAGW-5193 and NSF Grant No. ATM-8506646.

Appendix A: Eigenmodes of the Magnetospheric-Ionospheric System

The mutual inductance provides an intrinsically interesting modification to the dynamics that is seen by solving Eqs. (3) and (7) for $\dot{I}$ and $\dot{I}_1$. The solution requires the determinant

$$D = \mathcal{L}\mathcal{L}_I - M^2 \equiv \mathcal{L}\mathcal{L}_I(1 - \overline{m}^2) \tag{A1}$$

where $0 \leq \overline{m} \leq 1$. The matrix inversion for the solution is then

$$\begin{pmatrix} \dot{I} \\ \dot{I}_1 \end{pmatrix} = \frac{1}{\mathcal{D}} \begin{bmatrix} \mathcal{L}_1 & M \\ M & \mathcal{L} \end{bmatrix} \begin{bmatrix} V_{\rm sw} - V \\ V - V_I \end{bmatrix}. \tag{A2}$$

From the inverse (A2) we see that the effect of the mutual inductance is to *reduce* the effective values of the self-inductances. In particular, the diagonal components show that the effective inertial for I and I_1 are given by

$$\begin{aligned} \mathcal{L}^{\rm eff} &= \mathcal{D}/\mathcal{L}_1 = \mathcal{L}(1 - \overline{m}^2) \\ \mathcal{L}_1^{\rm eff} &= \mathcal{D}/\mathcal{L} = \mathcal{L}_1(1 - \overline{m}^2). \end{aligned} \tag{A3}$$

We have analyzed the linear eigenmodes of the 2-degree-of-freedom system (I, I_1, V, V_1) and find that in the dissipationless limit the frequencies ω are given by

$$\omega^4 - \mathcal{B}\omega^2 + \mathcal{D} = 0 \tag{A4}$$

with

$$\omega_\pm^2 = \frac{\mathcal{B} \pm \sqrt{\mathcal{B}^2 - 4\mathcal{D}}}{2} \tag{A5}$$

giving the high frequency oscillation

$$\omega_+^2 \cong \left(\frac{1}{C} + \frac{1}{C_1}\right) \frac{1}{\mathcal{L}_1(1 - \overline{m}^2)} \tag{A6}$$

involving the mutual inductance of the geotail and ionospheric circuits and the global low frequency oscillations

$$\omega_-^2 = \frac{1}{\mathcal{L}(C_1 + C)} \tag{A7}$$

in which $V_I \simeq V(t) \gg \omega_A M I$. In the low frequency component the cross-tail voltage V appears directly in the ionosphere while in the high frequency oscillations, characterized principally by the parameters of the plasma carrying the region 1 currents, the ionosphere voltage $V_I(t)$ lags the dawn-dusk geotail potential V in phase and is considerably small in value.

Appendix B: Connection to the Weimer Model

In the Weimer model as used by Klimas *et al.* (1994) the reaction of the ionosphere back onto the magnetotail is neglected. The reduced ionospheric equations are then

$$I_{\mathrm{AL}} = I_1 = C_I \frac{dV_I}{dt} + \Sigma_I V_I \tag{B1}$$

$$\mathcal{L}_I C_I \ddot{V}_I + \mathcal{L}_I \Sigma \dot{V}_I + V_I = V + M \frac{dI}{dt}. \tag{B2}$$

For a unit impulse input $V_0\delta(t)$ from the magnetotail this passive ionosphere response $V_s(p)$ is given by

$$\left(p^2 + \frac{\Sigma_I}{C_I} p + \omega_I^2\right) V_I(p) = \omega_I^2 V_0 \tag{B3}$$

where p is the Laplace transform variable. Here $\omega_I = (\mathcal{L}_I C_I)^{-1/2}$. Solving Eq. (B3) for the output voltage gives the response function

$$V_I(t) = V_0 \int \frac{\omega_I^2 e^{pt}}{(p-p_1)(p-p_2)} \frac{dp}{2\pi i} = \frac{\omega_I^2 V_0}{(p_2 - p_1)} \left(e^{p_2 t} - e^{p_1 t}\right). \tag{B4}$$

For real p_1 and p_2, we have

$$-1/p_1 = \text{rise time}$$

$$-1/p_2 = \text{decay time.}$$

In general p_1 and p_2 are given by

$$p_{1,2} = -\frac{\Sigma_I}{2C_I} \mp \left[\left(\frac{\Sigma_I}{2C_I}\right)^2 - \omega_I^2\right]^{1/2} \tag{B5}$$

and $\omega_I = (\mathcal{L}_I\, C_I)^{-1/2}$. Equation (B4) is the linear response function of the Weimer model used by Klimas *et al.* (1994). In Klimas *et al.* (1994) the choice was made of rise time $\tau_1 = 2\,\mathrm{min}$ and decay time $\tau_2 = 30\,\mathrm{min}$.

Table 1. Reference Parameters for Nonlinear Dynamics Model

$\beta_{\mathrm{sw}} = 0.25$	$u_0 = 6.0 \times 10^{-11}\,\mathrm{J}^{-1/2}\mathrm{s}^{-1}$
$\mathcal{L} = 40\,\mathrm{H}$	$I_c = 3.5 \times 10^7\,\mathrm{A}$
$C_{\mathrm{cps}} = 1.2 \times 10^4\,\mathrm{F}$	$\Delta I = 10^6\,\mathrm{A}$
$\Sigma = 40\,\mathrm{mho}$	$M = 1.1\,\mathrm{H}$
$\Omega_{\mathrm{cps}} = 1.6 \times 10^{24}\,\mathrm{m}^3$	$\mathcal{L}_1 = 12\,\mathrm{H}$
$\tau_{\parallel} = 10^3\,\mathrm{s}$	$C_1 = 10^3\,\mathrm{F}$
$v_{\mathrm{min}}^{\mathrm{sw}} = 30\,\mathrm{kV}$	$\Sigma_I = 4\,\mathrm{mho}$

REFERENCES

Akasofu, S.-I., The solar-wind magnetosphere energy coupling and magnetospheric disturbances, Planet. Space Sci. **28**, 495 (1980).

Ashour-Abdalla, M., L.M. Zelenyĭ, V. Peroomian, and R.L. Richard, Consequences of magnetotail ion dynamics, J. Geophys. Res. **99**, 14,891–14,916 (1994).

Baker, D.N., A.J. Klimas, T.I. Pulkkinen, and R.L. McPherron, Re-examination of the driven and unloading aspects of magnetospheric substorms, Adv. Space Res. **13**, 75 (1993).

Bargatze, L.F., D.N. Baker, R.L. McPherron, and E.W. Hones, Magnetospheric impulse response for many levels of geomagnetic activity, J. Geophys. Res. **90**, 6387–6394 (1985).

Birn, J., and M. Hesse, Details of current disruption and diversion in simulations of magnetotail dynamics, J. Geophys. Res. **101**, 15,345–15,358 (1996).

Blanchard, G.T., and R.L. McPherron, A bimodal representation of the response function relating the solar wind electric field to the AL index, Adv. Space Res. **13**, (4)71 (1993).

Blanchard, G.T., and R.L. McPherron, Analysis of the linear response function relating AL to VBs for individual substorms, J. Geophys. Res. **100**, 19,155–19,165, (1995).

Braginskii, S.I., *Reviews of Plasma Physics*, (Consultants Bureau, New York, 1965), Vol. I, pp. 250–253.

Brecht, S.H., J.G. Lyon, J.A. Fedder, and K. Hain, A time dependent three-dimensional simulation of the Earth's magnetosphere: Reconnection events, J. Geophys. Res. **87**, 6098 (1982).

Fedder, J.A., and J.G. Lyon, The Earth's magnetosphere is $165\,R_E$ long: Self-consistent currents, convection, magnetospheric structure, and processes for northward interplanetary magnetic field, J. Geophys. Res. **100**, 3623–3635 (1995).

Goertz, C.K., L-H. Shan, and R.A. Smith, Prediction of geomagnetic activity, J. Geophys. Res. **98**, 7673 (1993).

Hernández, J., T. Tajima, and W. Horton, Neural net forecasting for geomagnetic activity, Geophys. Res. Lett. **20**, 2707–2710 (1993b).

Hernández, J., A. Vannucci, T. Tajima, Z. Lin, W. Horton, and S.C. McCool, Neural network prediction of some class of tokamak disruption, Nucl. Fusion **36**, 1009–1017 (1996).

Hill, T.W., Magnetic merging in a collisionless plasma, J. Geophys. Res. **80**, 4689–4699 (1975).

Horton, W., and T. Tajima, Linear theory of driven reconnection, J. Geophys. Res. **93**, 2741–2748 (1988).

Horton, W., and T. Tajima, Decay of correlations and the collisionless conductivity in the geomagnetic tail, Geophys. Res. Lett. **17**, 123–126 (1990).

Horton, W. and T. Tajima, Collisionless conductivity and stochastic heating of the plasma sheet in the geomagnetic tail, J. Geophys. Res. **96**, 15,811–15,829 (1991).

Horton, W., and I. Doxas, A low-dimensional energy conserving state space model for substorm dynamics, J. Geophys. Res. **101A**, 27,223–27,237 (1996).

Hoshino, *et al.*, "Origin of hot and high speed plasmas," Adv. Space Res. (in press) (COSPAR Review paper).

Iijima, T., and T.A. Potemra, Large-scale characteristics of field-aligned currents associated with substorms, J. Geophys. Res. **83**, 599–615 (1978).

Klimas, A.J., D.N. Baker, D.A. Roberts, D.H. Fairfield, and J. Büchner, A nonlinear analog model of geomagnetic activity, J. Geophys. Res. **97**, 12,253 (1992).

Klimas, A.J., D.N. Baker, D. Vassiliadis, and D.A. Roberts, Substorm recurrence during steady and variable solar wind driving: Evidence for a normal mode in the unloading dynamics of the magnetosphere," J. Geophys. Res. **99**, 14,855 (1994).

Klimas, A.J., D. Vassiliadis, D.N. Baker, and D.A. Roberts, The organized nonlinear dynamics of the magnetotail, J. Geophys. Res. **101**, 13089.

Luciani, J.F., P. Mora, and J. Virmont, Nonlocal heat transport due to steep temperature gradients, Phys. Rev. Lett. **51**, 1664–1667 (1983).

Lui, A.T.Y., A. Mankofsky, C.-L. Chang, K. Papadopoulos, and C.S. Wu, A current disruption mechanism in the neutral sheet: A possible trigger for substorm expansions, Geophys. Res. Lett. **17**, 745 (1990).

Lyons, L.R., and T.W. Speiser, Evidence for current sheet acceleration in the geomagnetic tail, J. Geophys. Res. **87**, 2276 (1982).

Lyons, L.R., A new theory for magnetospheric substorms, J. Geophys. Res. **100**(A10), 19,069–19,081 (1995).

Lyons, L.R., Substorms: Fundamental observational features, distinction from other disturbances, and external triggering, J. Geophys. Res. **101**(A6), 13,011–13,025 (1996).

Nishida, A., Geomagnetic D_p 2 Fluctuations and Associated Magnetospheric Phenomena, J. Geophys. Res. **73**, 1795–1803 (1968).

Ogino, T., An MHD Simulation of the IMF Control on Magnetotail, to appear in *Proceedings of the Chapman Conference, Kanazawa, 1996.*

Perrault, P. and S.-I. Akasofu, A study of magnetic storms, Geophys. J.R. Astron. Soc. **54**, 547 (1978).

Reiff, P.H., R.W. Spiro, and T.W. Hill, Dependence of polar cap potential drop on interplanetary parameters, J. Geophys. Res. **86**, 7639–7648 (1981).

Robinson, R.M., R.R. Vondrak, K. Miller, T. Dabbs, and D. Hardy, On calculating ionospheric conductances from the flux and energy of precipitating electrons, J. Geophys. Res. **92**, 2265–2569 (1988).

Rostoker, G., J.C. Samson, F. Creutzberg, T.J. Hughes, D.R. McDiarmid, A.G. McNamara, A. Vallance Jones, D.D. Wallis, and L.L. Cogger, Canopus—A ground-based instrument array for remote sensing the high latitude ionosphere during the ISTP/GGS program, Space Sci. Rev. **71**, 743–760 (1995).

Smith, J.P., and W. Horton, "Analysis of the Bi-modal Nature of Solar Wind—Magnetospheric Coupling," IFS Report #788, submitted to J. Geophys. Res. (1997).

Steinolfson, R.S., and R.M. Winglee, Energy storage and dissipation in the magnetotail during substorms. 2. MHD simulations, J. Geophys. Res. **98**, 7537 (1993).

Terasawa, T., Numerical study of explosive tearing mode instability in a one-component plasma, J. Geophys. Res. **86**, 9007 (1981).

Tsyganenko, N.A., A magnetospheric magnetic field model with a warped tail current sheet, Planet Space Sci. **37**, 5 (1989).

Usadi, A., A. Kageyama, K. Watanabe, and T. Sato, A global simulation of the magnetosphere with a long tail: Southward and northward interplanetary magnetic field, J. Geophys. Res. **98**, 7503–7517 (1993).

Winglee, R.M., and R.S. Steinolfson, Energy storage and dissipation in the magnetotail during substorms. 1. Particle simulations, J. Geophys. Res. **98**, (1993).

Yang, Y.S., R.W. Spiro, and R.A. Wolf, Generation of region 1 current by magnetospheric pressure gradients, J. Geophys. Res. **99**, 223–234 (1994).